Final Report 1998-25

An Automatic Visibility Measurement System Based On Video Cameras

Technical Report Documentation Page

1. Report No.	2.	3. Re
MN/RC - 1998-25		PB99-123473

4. Title and Subtitle	5. Report Date
AN AUTOMATIC VISIBILITY MEASUREMENT SYSTEM BASED ON VIDEO CAMERAS	September 1998
	6.

7. Author(s)	8. Performing Organization Report No.
Taek Mu Kwon	

9. Performing Organization Name and Address	10. Project/Task/Work Unit No.
University of Minnesota - Duluth Department of Electrical and Computer Engineering 10 University Drive Duluth, Minnesota 55812	11. Contract (C) or Grant (G) No. (C) 74708 TOC # 10

12. Sponsoring Organization Name and Address	13. Type of Report and Period Covered
Minnesota Department of Transportation 395 John Ireland Boulevard Mail Stop 330 St. Paul, Minnesota 55155	Final Report - 1996 to 1998
	14. Sponsoring Agency Code

15. Supplementary Notes

16. Abstract (Limit: 200 words)

The Minnesota Department of Transportation (Mn/DOT) conducted a two-year study on visibility measurement methods using video cameras. This report describes the study's theoretical basis, practical methods, and experimental results.

Among several methods and algorithms developed, the edge decay model along with a proper threshold technique worked best for evaluating daytime visibility. This approach estimates the distance where an object of specified size and shape is no longer distinguishable from the background in terms of edge information. For night time, a constant light source is required to evaluate visibility. Researchers developed a light diffusion model that follows an exponential decay curve.

Researchers determined that the volume of light diffused out of the original source logarithmically correlates to visibility. Mn/DOT implemented day and night algorithms in the field and evaluated them using manual measurements. For daytime, visibilities measured using the edge decay model closely approximated the manual measurements on all types of weather. Unreliability of manual measurements at night made night-time evaluation very difficult. However, research verified that the trend of visibility change obtained by the proposed approach closely approximates the trend of manual measurements.

17. Document Analysis/Descriptors		18. Availability Statement
visibility video camera visual range	scattering effect stopping distance	No restrictions. Document available from: National Technical Information Services, Springfield, Virginia 22161

19. Security Class (this report)	20. Security Class (this page)	21. No. of Pages	22. Price
Unclassified	Unclassified	66	

An Automatic Visibility Measurement System Based on Video Cameras

Final Report

Prepared by

Taek Mu Kwon, Ph.D

Department of Electrical and Computer Engineering
University of Minnesota, Duluth Campus
Duluth, MN 55812

September 1998

Prepared for the

Minnesota Department of Transportation
Duluth Office and
Office of Research Administration
200 Ford Buildings Mail Stop 330
117 University Avenue
St. Paul, Minnesota 55155

ACKNOWLEDGEMENTS

The author expresses appreciation to the Office of Research Administration and Mn/DOT District -1 for financial and manpower support for this research. Special thanks to Mr. Edward Fleege of Mn/DOT for his tireless help on all phases of the project. Several maintenance engineers at the Mn/DOT Duluth Office also provided valuable assistance. Thanks also to Mr. Tim Garret of Castle Rock Consulting Company for providing me large collection of video data from the previous visibility study.

CONTENTS

LIST OF TABLES

LIST OF FIGURES

EXECUTIVE SUMMARY

This report describes the project entitled "An Automatic Visibility Measurement System Based on Video Cameras" which was supported by the Mn/DOT MORE fund. The main goal of this project was to develop a new technique that could measure visibility using video cameras. This design goal was motivated by the fact that video cameras are used extensively in transportation applications, and using the same hardware for visibility evaluation could provide a cost effective solution. In Minnesota, areas with visibility problems identified by Mn/DOT have video cameras already or will be in place. As an initial step, literature on visibility measurement methods was extensively reviewed. The research team found that no practical and reliable techniques to measure visibility using video cameras exist at the present time. Hence, this research embarked on developing a new set of algorithms for daytime and nighttime visibility using video cameras which are practical and reliable enough for field use.

The main algorithm developed for daytime is based on the concept that edge information decreases with distance along with the line of sight. At some point, edges will become extinct. The distance to the point of extinction is the visibility, since object of given characteristic is no longer distinguishable. This approach is significantly different from the traditional approach (i.e. contrast based Koschmieder rule) in that we actually measure how far we can recognize an object. Therefore, the parameter obtained by this new approach is close to the actual visibility that a typical human observer may perceive. For nighttime, the amount of volume diffused out of a constant light source was used. This diffused volume is then modeled using an exponential decay rule, from which an extinction coefficient is derived.

In order to evaluate the algorithms developed, two types of real world test beds were used. The first test bed was based on a set of real-world highway data collected over a one-year period. This data set was provided by the Castle Rock Consulting Co. which conducted a study on performance comparison of commercially available visibility meters against manual measurements. The second test bed was directly performed in the field by comparing video visibility with manual

measurements. This testing was conducted over a period of two years. The test result showed that the performance of the present video based approach in daytime is as good as the commercially available scattering based instruments in fog and better in snow as long as the video images are reliable. For nighttime, manual measurements were extremely difficult. Therefore, the algorithm was only tuned using very rough estimates. A further study is recommended for night time.

I. INTRODUCTION

Visibility conditions are affected by the structure and elements of the atmosphere, such as fog, snow, wind, dust, and other adverse conditions. It is loosely defined as the greatest distance at which an object of specified characteristics can be seen and detected with the naked eye [1,2,8]. It is expressed in meters or yards, or at greater ranges, in kilometers or miles. At night, it is determined by measuring the distance from a point of light of a given intensity to the point where the light source is just noticeable.

Visibility information provides an identifiable target distance from which we can derive safe speed limits by incorporating breaking distances per speed. Consequently, visibility is one of the important determinants for safe driving.

Traditionally, visibility has been evaluated manually or by using commercial visibility instruments. The latter are constructed based on the principle of measuring forward or backward light-scattering effects. The main advantage of the scattering based instruments is the capability of evaluating nighttime visual range without modification from the daytime setup. However, several drawbacks should be noted and are listed below:

- Visibility is not only reduced by the scattering effect but also by absorption. Hence measuring scattering alone accounts for only a partial view of the atmospheric visibility effects.
- Visibility measured by the scattering instruments represents a single spot; thus, covering a large area requires many repeated installations, which can greatly increase the overall cost.
- Scattering based instruments show a high margin of error under snow and rain while they are relatively accurate under fog. This is due to a less significant relation of visibility to the scattering effect under snow or rain. This observation was pointed out by Castle Rock's study [5] whereby several commercial visual-range sensors failed to recognize low visibility caused by snow. This inconsistency of errors could pose a problem in practical

implementation because it may require different calibrations under different weather conditions.

- Scattering instruments only measure visual-range, not visibility. This means that visibility perceived by human eye could be significantly different from the visual range measured by the scattering based instruments.
- There are no easy ways to verify the correctness of the measured visual range. Video cameras are frequently used to verify correctness of the measurements, but it greatly increases the instrumentation and communication cost.
- The scattering based instruments are relatively expensive.

The above list is not an exclusive list, but are the items of concern when scattering based commercial instruments are used as the visibility sensor in the field. As an alternative to the scattering-based instruments, video cameras offer an attractive solution for evaluating visibility. The reasons are summarized below, and are the subject of this study in which we will explore and develop useful techniques.

- Since many video cameras are already installed and used for transportation applications, it provides a low cost solution for visibility evaluation if the same hardware is used.
- Video cameras display view along the line of sight instead of a single spot, so that it represents a large area and provides an estimate less prone to drastic local errors.
- The camera lens system has the same structure as the lens system of human eye. Thus, it provides an opportunity for measuring perceptual visibility.
- Video information on the actual scene can be obtained as a byproduct of the approach, which provides an opportunity to verify the measured visibility by manual inspection.
- In Minnesota, all areas with visibility problems have video cameras already in place.

The above are a list of the advantages that the video camera based approach has over the scattering based approach. However, there are some disadvantages that should be noted. These include: 1) images can be distorted by dirty lenses; 2) images are sensitive to lighting conditions; 3) objects are not identifiable at night; 4) images can be blurred by poor focusing.

Despite some difficulties associated with video cameras, the advantages clearly outweigh the disadvantages. It is essentially the ultimate approach to resolve the visibility issue, because the information seen by the human eye has the same principle as the information generated by a video camera. Therefore, we have an opportunity to explore the various methods and principles that could derive what a human observer may perceive the visibility.

II. VISIBILITY CONCEPTS AND TERMINOLOGY

Measuring visibility is inherently difficult because it involves measuring the perceptual process of human subjects, i.e. object recognition. As of today, it is still not well understood how we recognize objects. For example, identification rate can be increased with prior knowledge about the object, and quantization of such phenomenon is very difficult. In order to avoid such problems scientists evaluate another parameter called the *visual range* in place of visibility. This is defined by a just minute difference of a black target against the horizon measured by the contrast ratio. In this concept, visual range is only evaluated by measuring the atmospheric attenuation of contrast, and scientists and engineers are no longer concerned about human perception. The following summarizes the basic terminologies related to visual range [1,13].

A. Daytime Visual Range

Daytime visual range is evaluated based on an assumed minimal contrast ratio (0.02 - 0.05, we adopt 0.05 based on the recommendation by the National Bureau of Standards [8]) for a black target of "reasonable" size silhouetted against the horizon viewed by a typical human eye. A reasonable size by this definition is an object that subtends an angle of 0.5-1.0 degree of arc from the observer. Under these conditions, visual range V is estimated from the average extinction coefficient σ using the Koschmieder equation:

$$V = \frac{3.0}{\sigma} \qquad (1)$$

where V is the visual range in meters if σ is in m^{-1}.

B. Nighttime Visual Range

The nighttime visual range is evaluated based on minimum amount of light falling on the observer's eye which produces a recognizable sensation of brightness. It is governed by the Allard's law, which is expressed by

$$E_{th} = \frac{Ie^{-\sigma V}}{V^2} \qquad (2)$$

where E_{th} is the threshold illuminance detected at the visual range V by a light source of intensity I.

C. Meteorological Range

Meteorological Range is an empirically consistent measure of visual range; a concept developed to eliminate from consideration of the threshold contrast and adaptation luminance, both of which vary from observer to observer. For practical purposes one may calculate meteorological range in the same manner as the daytime visual range relation given in Eq. (1). This formulation satisfies the requirements of meteorologists since it yields a one-to-one correlation with atmospheric transmittance, and a change from day to night does not produce a change in the visual range.

D. Runway Visual Range

The maximum distance along the runway at which the runway lights are visible to a pilot after touchdown. Runway visual range may be determined by an observer located at the end of the runway, facing in the direction of landing, or by means of a transmissometer installed near the

end of the runway.

E. Recommended Accuracy Requirements

The accuracy requirements recommended for visibility measurements are specified in World Meteorological Organization (WMO) Publication No. 8, "Guide to Meteorological Instruments and Methods of Observation," 5th Ed., 1983. It includes the error requirements for aeronautical and meteorological applications, but does not include the requirements for ground level transportation applications. The requirements for runway visual range may be closely related to the highway transportation applications, in which the allowable errors are defined as ±25 meters up to 150 meters; ±50 meters between 150 to 500 meters; and ±100 meters between 500 to 1000 meters, and ±200 meters above 1000 meters.

III. THEORETICAL DERIVATION OF VISUAL RANGE

This section presents theoretical derivations of visual-range algorithms studied in this project. The fundamental theory of visual range based on contrast is reviewed. New approaches are derived from the basic theorem.

A. Basic Principles of Visual Range Based on Contrast

Let the luminance of a target be B_t and the horizon background surrounding the target be B_h, then the contrast C is defined as

$$C = \frac{B_t - B_h}{B_h}. \tag{3}$$

With this definition, contrast may be either positive or negative, with negative meaning that the target is less luminous than the background. According to Duntley [4], the contrast ratio is governed by the following rule:

$$\frac{C}{C_0} = e^{-\sigma d} \tag{4}$$

where C_0 is the inherent contrast against sky (i.e the contrast measured at the target), C is the apparent contrast of the target observed from distance d, and σ is the light attenuation coefficient (called the extinction coefficient). Visual range V is then defined at the distance where the contrast ratio falls down to $C/C_0 = \epsilon_0 = 0.05$;

$$0.05 = e^{-\sigma V} \tag{5}$$

If σ is obtainable through a transmissometer, visual range is simply computed from Eq. (5) as:

$$V = \frac{\ln \varepsilon_0}{-\sigma} = \frac{3.0}{\sigma} \tag{6}$$

If the contrast ratio C/C_0 at distance d is measurable, its visual range is computed by substituting σ in Eq. (4) to Eq. (6), i.e.

$$V = \frac{d \cdot 3.0}{\ln \frac{C_0}{C}} \tag{7}$$

B. Dual Target Approach

Daytime Visual Range

Direct measurement of inherent contrast C_0 in Eq. (7) is not simple, because the contrast must be measured against sky which is infinite while the measurement has to incorporate the dependency of contrast in light-intensity and weather conditions. To avoid such difficulty we develop a dual-target approach that removes the requirement of measuring the inherent (reference) contrast C_0. The basic principle of theory is derived by assuming that two targets are set up at distances d_1 and d_2 against horizon as shown in Fig. 1. At the observation point of the diagram, an observer or an instrument measures the contrast of the two targets. Let the measured contrasts be C_1 and C_2 for each target, respectively. Then, using Eq. (4) we have

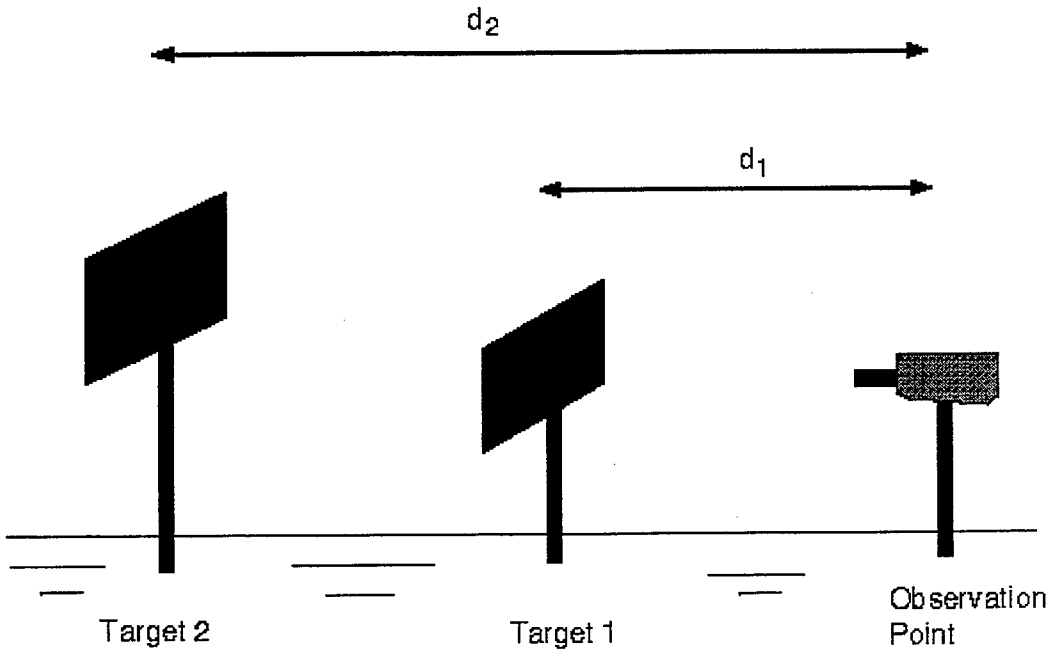

Figure 1: Dual target setup for daytime visual range.

$$\sigma = \frac{1}{d_1} \ln \frac{C_0}{C_1} \tag{8}$$

$$\sigma = \frac{1}{d_2} \ln \frac{C_0}{C_2} \quad . \tag{9}$$

Solving for C_0 from Eqs. (8) and (9) gives,

$$\ln C_0 = \frac{d_2}{d_2 - d_1}\ln C_1 - \frac{d_1}{d_2 - d_1}\ln C_2 . \qquad (10)$$

Finally, substituting Eq. (10) to Eq. (7) yields the visual range we wish to calculate without using the reference contrast:

$$V = \frac{(d_2 - d_1)(-\ln \varepsilon_0)}{\ln \frac{C_1}{C_2}}. \qquad (11)$$

Notice from Eq. (11) that the formula consists of no C_0 and all easily measurable values. Moreover, since the contrast values only appear as a ratio (i.e. C_1/C_2), any contrast measurements are valid as long as the lighting conditions are consistent for both targets. In other words, brightness change during the day or automatic iris adjustments will not influence the accuracy of the visibility computation as long as the both targets are under the same atmospheric conditions. On the other hand, we learned that creating such condition is hard to obtain. For example, light attenuation coefficients of atmosphere can be inconsistent within a short distance.

In our case, since the contrasts of two targets are measured from a video image, it is simultaneously recorded in the same image. Hence, it is temporally consistent as well as spatially (i.e. the photo-cells at each pixel location is consistent). However, since atmospheric inconsistency can not be controlled, a short distance between two targets are recommended in order to minimize the atmospheric inconsistency.

It should be noted that a video image is a collection of pixel values some of which are saturated to upper or lower limits. Grey scale resolution of each pixel is generally limited to 256 levels (8-bit). Because of these limits, directly computing visual range using Eq. (11) is prone to a large

error depending on the resolution and the linearity of luminance to the pixel value. Consequently, some adjustments must be made to Eq. (11) to minimize the effect; the following is suggested:

$$V = \frac{\beta}{\ln C_1 - \ln C_2} \tag{12}$$

where β is a constant factor that must be calibrated through manual verification of visibility. This adjustment is necessary to establish a mapping relation between the pixel value and the actual luminance. In Eq (12), if the contrast of target-2 is reduced with respect to target-1, the visibility is reduced proportionally in a log scale. This follows the Duntley's law in Eq. (4).

Nighttime Visual Range

Nighttime visual range is defined as the greatest distance at which a point of light-source of the given candle-power can be perceived at night by an observer under the given atmospheric condition. Nighttime visual range is limited by atmospheric attenuation of luminous flux density as described by the Allard's law in Eq. (2). Let E_{th} be the luminance threshold that is just noticeable from the visual range V, then rewriting Eq. (2) gives

$$\frac{E_{th}}{I} V^2 = e^{-\sigma V} \tag{13}$$

The nighttime visual range [2] is then simply derived by solving for V from Eq.(13), i.e.,

$$V = \frac{1}{\sigma}(\ln \frac{I}{E_{th}} - 2 \ln V) \tag{14}$$

Unfortunately, the relationship in (14) is impractical for visual-range computation, since the light attenuation coefficient σ is unknown (must be measured) and the luminance threshold E_{th} must be adjusted under different lighting conditions. Therefore, we develop a dual-target approach similar to that of the daytime visual-range, which does not require to know either E_{th} or σ. Suppose that two targets are set up at distances d_1 and d_2 with an identical light intensity (unfocused light source) as shown in Fig. 2. Let the luminance of the two targets detected at the observation point be E_1 and E_2, respectively. Then, for each target, the following relations hold:

$$E_1 = \frac{I}{d_1^2} e^{-\sigma d_1} \tag{15}$$

$$E_2 = \frac{I}{d_2^2} e^{-\sigma d_2} \tag{16}$$

Solving for σ from Eqs. (15) and (16) gives

$$\sigma = \frac{1}{d_1 - d_2} \ln \frac{E_2 d_2^2}{E_1 d_1^2} \tag{17}$$

Notice that E_1, E_2, d_1, and d_2 are all known or measurable values. This means that we can derive the light attenuation of atmosphere if two identical light sources at different locations are available. Using Eqs (17) and (14), we arrive at a measurable nighttime visual range as:

$$V = \frac{(d_1 - d_2)}{\ln \frac{E_2 d_2^2}{E_1 d_1^2}} (\varepsilon - 2 \ln V) \tag{18}$$

where ϵ is determined through field experiments.

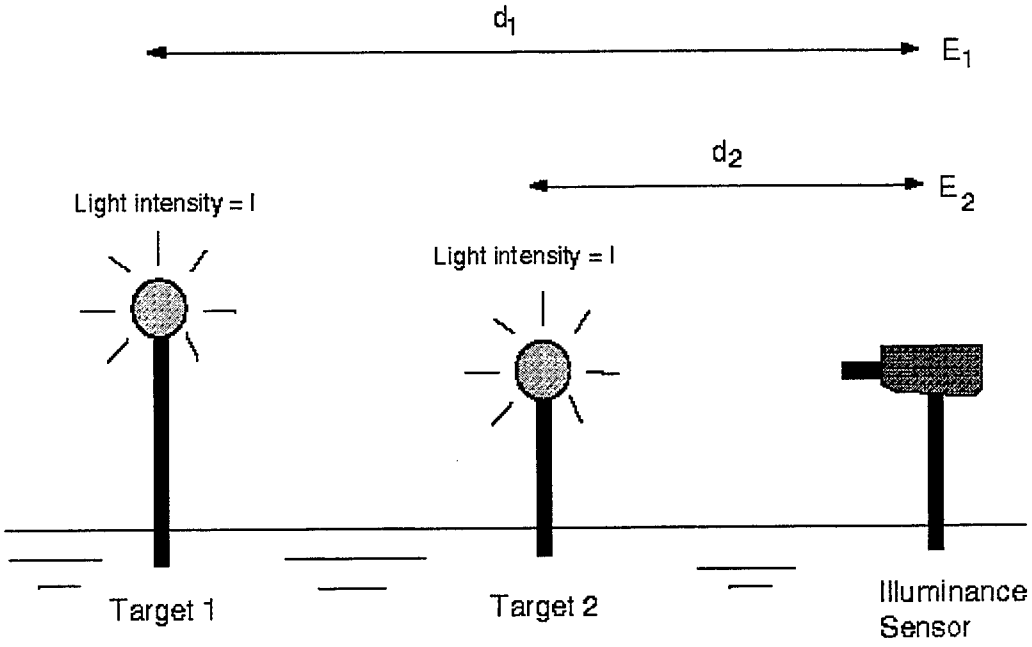

Figure 2: Dual target setup for nighttime visual range evaluation.

Further simplification is necessary in order to remove the recursive relation in Eq. (18) , i.e.

$$V \approx \frac{(d_1 - d_2)\alpha}{\ln \frac{E_2 d_2^2}{E_1 d_1^2}} \tag{19}$$

where α is a multiplication factor that is required by just noticeable light source. If sufficient data can be collected, a sophisticated model can be further developed using the key variables. Let the variables be

$$D_d = |d_1 - d_2|$$

$$D_E = |\ln E_1 - \ln E_2|$$

The visibility is then conveniently modeled through an Nth order polynomial, i.e.

$$V = a_0 + a_1 D_d + b_0 + b_1 D_E + b_2 D_E^2 + \ldots + b_N D_E^N \qquad (20)$$

The coefficients are commonly solved using iterative methods such as a least squares method.

Comments on Night Visibility

In reality, measuring visibility at night is extremely challenging whether it is manual or automated system. Middleton best describes this difficulty in his famous book, *Vision Through the Atmosphere* [2] as follows: "If observation in daytime have their difficulties, these are negligible in comparison with those encountered at night."

Ideally, we want to have a camera that gives a parameter linear to the light intensity of targets. However, video cameras in general are designed to work best for capturing daytime images and not for detecting light-intensity at night. We found that the pixels of the video camera tend to saturate quickly against any light source due to the high contrast against dark background at night. Therefore, we believe that the method developed in Subsection III.B is appropriate for the sensors that exhibit a large linear region against light intensity. In the next section, we show a new approaches that are more appropriate for video cameras.

C. A New Approach Based on Edge and Diffusion Models for Video Images

Daytime Visibility Derivation Using Edge Information

This approach utilizes the perceptual degradation of an image along the line of sight that corresponds to actual distances from the observation point. For example, tree lines or fence lines along the highway can form a continuous degradation model along the straight line of sight, from which extinction of contrast may be detected at some point along that line. To be more specific, consider the sample road scene shown in Figure 3, where the right side along the edge strip is chosen for processing. Let the *localized contrast* along the ideal line be denoted *C(d)*, then it is an exponentially decreasing function due to the contrast reduction principle in Eq. (4):

$$C(d) = k \cdot C_0 e^{-\alpha d} \tag{21}$$

where k is a scaling factor. It should be mentioned that this relation is a rough approximation of real contrast due to the limits imposed on each pixel and existence of non-ideal continuous targets.

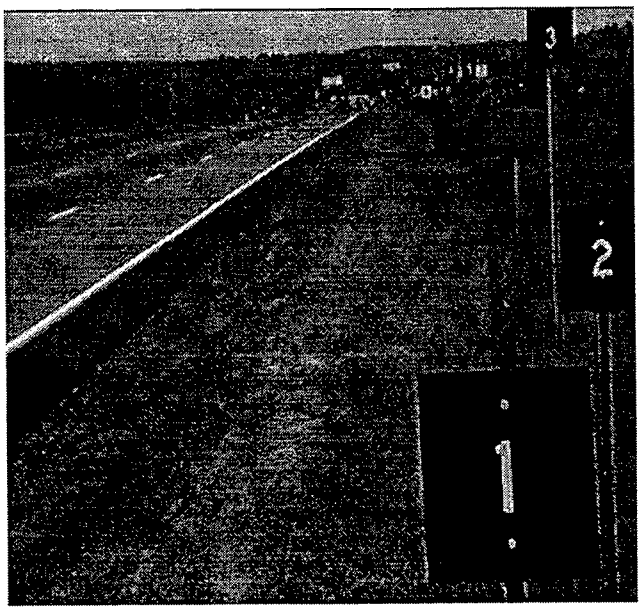

Figure 3: Sample road scene.

For the evaluation of localized contrasts at pixel location *(i,j)*, the following formulation can be used by incorporating the contrast definition given by Eq. (3):

$$C(i,j) = \frac{p(i,j) - p_{av}}{P_{av}} \tag{22}$$

where $p(i,j)$ denotes the pixel value at location *(i,j)* and p_{av} is the average of the pixel values surrounding the location *(i,j)*. At this point, we may depart from the traditional computation of contrast. It is well known that the human visual system inherently utilizes edge information for object recognition, as is readily evidenced by the way we recognize cartoon pictures. Hence, it is more logical to utilize the degree of edge information for visibility evaluation than the contrast by luminance. Thus, without loss of generality, we replace the contrast computation in Eq. (22) with an edge operator. A well known edge operator that has been successfully used in many applications is the Sobel operator [6], which is given by

$$S(m,n) = (d_x^2 + d_y^2)^{1/2} \tag{23}$$

where

$$\begin{aligned} d_x &= (p(m-1,n-1) + 2p(m,n-1) + p(m+1,n-1)) - \\ &\quad (p(m-1,n+1) + 2p(m,n+1) + p(m+1,n+1)), \\ d_y &= (p(m+1,n-1) + 2p(m+1,n) + p(m+1,n+1)) - \\ &\quad (p(m-1,n-1) + 2p(m-1,n) + p(m-1,n+1)). \end{aligned}$$

It should be mentioned that other edge operators may be equally eligible for this application, i.e., the performance difference by the choice of different edge operators is negligible in this case.

The Sobel values essentially approximate the gradient of an image by a difference operator. Notice that both the contrast in Eq. (22) and the gradient in (23) include differential terms. This implies that both in essence represent the same characteristics, i.e. gradient but in different scale. Next we map the two-dimensional Sobel data to a one dimensional representation by selecting a maximum edge from each orthogonal direction along the line of sight. The reason for this is to construct the model based on the best edges. Let the maximum edge values along the line-of-sight be represented by $\hat{S}(d)$. We experimentally found that $\hat{S}(d)$ follows the following exponential rule:

$$\hat{S}(d) = \frac{K_1}{1 + e^{\alpha(d - d_0)}} + K_0 \qquad (24)$$

where d is the distance from camera to target, and α is a parameter that controls the slope of the curve, and d_0 is the displacement of sloped region. Finally visibility is determined at the threshold $\hat{S}_{th}$ as

$$V = d_0 - \frac{1}{\alpha} \ln\left(\frac{K_1}{\hat{S}_{th} - K_0} - 1\right). \qquad (25)$$

This new approach is particularly suitable for measuring visibility on highways, since objects along the straight line-of-sight usually exist (such as tree lines, fence, side ditches), or artificial targets can be easily placed. One particular advantage of this method is that it is minimally sensitive to the types of targets. For example, if we choose the tree line along the roadway, no maintenance of targets will be required, and will be free of errors due to minor target damages or distortions.

Nighttime Visual Range

Since nighttime visual range is defined by a distance where a light source is just noticeable, the availability of a light source and a light-intensity meter is prerequisite for nighttime visual-range measurement. In this project, the average pixel value of a light source in a video image was initially used as the intensity. After many trial and error of using a video-camera for a light-intensity measurement, we recognized that directly measuring light intensity from video images cannot work. This is due to the fact that, characteristically, many video cameras use charge coupled devises (CCD), tending to quickly saturate at the location of light source. This quick saturation was caused by the very high contrast existing between the light source and the total dark background, leaving only a very narrow linear range. Therefore, we concluded that a new approach must be developed for nighttime visual-range if we are going to use a video camera.

After many experiments, we found one characteristic that closely relates to light intensity which is useable for night visibility. This parameter was the amount of diffused volume out of the saturated region of the light source. According to our observation, the diffusion volume was increased as visibility decreased. This phenomenon is clearly shown in Figs. 4- 6 and 7-9 where Figs. 4-6 show a good visibility example and Figs. 7-9 show a bad visibility example (about 200 meters). The three-D graphs show the light intensity profile, and the two-D graphs show the cross-section. Notice that Fig. 5 has almost no diffused lights while Fig. 8 has a lot of diffused lights. If we plot the cross-section of the diffused area, it follows exponential curves as shown in Figs. 6 and 9. In general, the following relation holds:

$$F(\eta, d) = F_0 e^{-\eta d} . \tag{26}$$

We will call η as the diffusion coefficient and F as the diffusion curve. In order to relate Eq. (26) with the traditional formulation, let's assume that we measured an identical light source under two different extinction coefficients, σ_1 and σ_2. Let the measured light intensities at a distance R

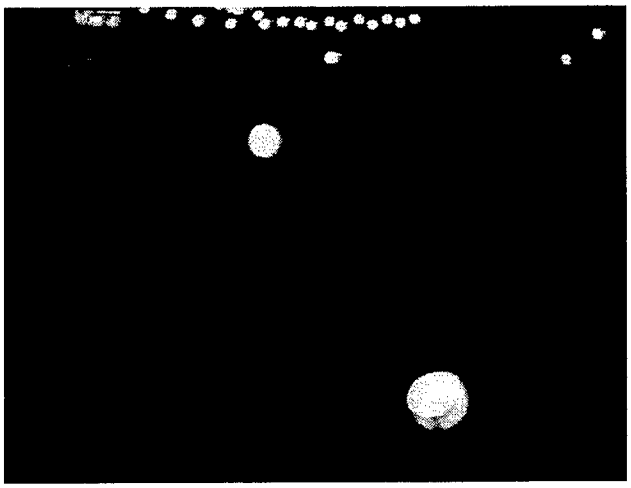

Figure 4: Image of a good visibility night.

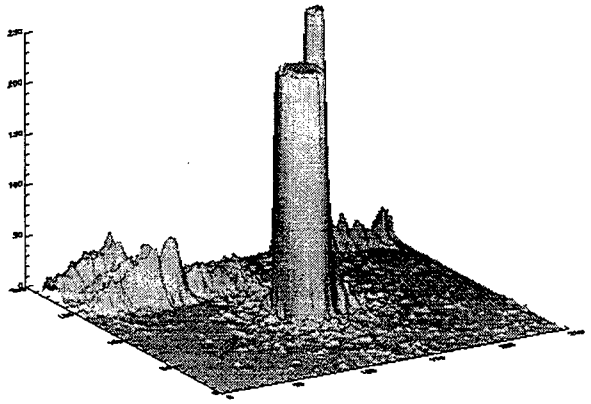

Figure 5: 3-D plot of the segmented light target from Figure 4.

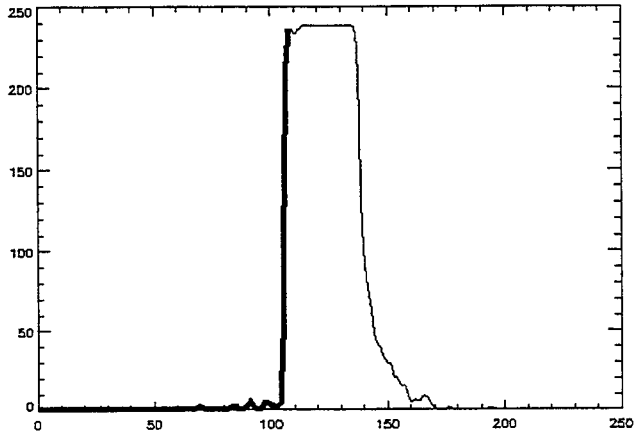

Figure 6: 2-D cross-section plot of Figure 5.

Figure 7: Image of a low visibility night.

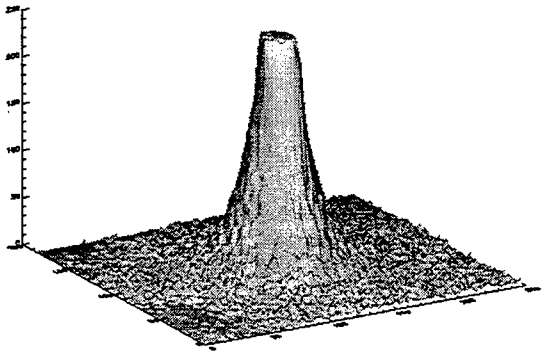

Figure 8: 3-D plot of the segmented light target from Figure 7.

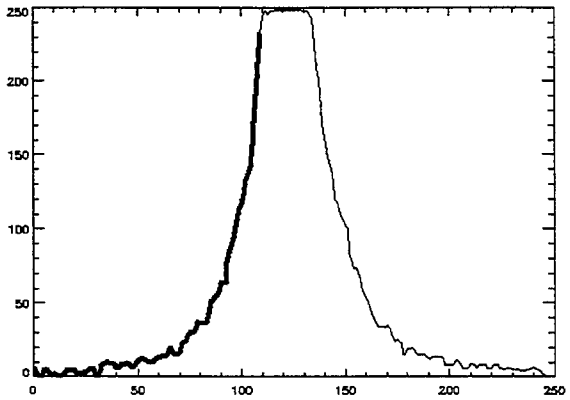

Figure 9: 2-D cross-section plot of Figure 8.

be E_1 and E_2, respectively to σ_1 and σ_2. Then, the following relation can be derived using the classical Allard's law in Eq. (2):

$$E_1 - E_2 = \frac{E_0}{R^2}(e^{-\sigma_1 R} - e^{-\sigma_2 R}) . \tag{27}$$

Now, let's further assume that we derived two diffusion curves on the same light source under the same extinction coefficients σ_1 and σ_2 as in Eq. (27). Let the diffusion values measured be F_1 and F_2 at distance d, then we have,

$$F_1 - F_2 = \frac{F_0}{R^2}(e^{-\eta_1 d} - e^{-\eta_2 d}) \tag{28}$$

where η_1 and η_2 are the computed diffusion coefficients using the basic diffusion model in Eq. (26). From Eqs. (27) and (28), we have the following relation

$$\eta d = \sigma R \tag{29}$$

Since both d and R represent distances, we can derive general visual range by setting a threshold E_{th} as the reference. In conclusion, nighttime visual range holds the following relation with respect to the diffusion coefficient:

$$V \propto \eta \tag{30}$$

or can be computed by

$$V = k \cdot \eta \tag{31}$$

where k is a constant scaling factor. This linear relation holds in most of the visual ranges. However, if some areas do deviate from this linear relation, we can always introduce a polynomial mapping function, i.e.

$$V = f_p(\eta) \tag{32}$$

where $f_p(\cdot)$ is a polynomial function.

IV. IMPLEMENTATION

This section describes implementation of the theory into practice where various hardware, software, and communication issues are involved.

A. Selection of Video Cameras

With the advances in imaging technologies, video cameras can capture sufficient resolution of images suitable for visibility evaluation. Ideally, we would like to have a camera that can simulate the characteristics and functions of human eye. As a general rule, cameras with the following features are recommended:

- *Auto iris.* Iris automatically controls the amount of light. It is generally controlled through the exposer time in CCD Cameras.

- *High resolution.* The human eye has much higher resolution than present video camera resolutions. One way of overcoming this problem is through the use of telephoto lenses to compensate the lack of resolution in the video camera.
- *Back light compensation.* An automatic back light compensation function is desirable to minimize the drastic contrast drop at the objects when the camera is against sunlight.
- *Defrost heater and fan.* During cold winter weather or damp summer days, frost or fog on the lens can severely degrade the quality of an image. Heaters and cooling fans are required to defrost or defog the camera lens.
- *Automatic lens cleaning function.* Snow, mud, dust, etc., on the lens can severely distort the image. An automatic cleaning function or a protective mechanism is required to maintain the lens clean.

B. Target Design

How to design the target model is important, but it is not a critical factor to the performance as long as some common senses described below are applied. The following guidelines are recommended.

- At least one target must include a constant light source for night visibility.
- The size of the targets must appear approximately the same size in the video image. This is achieved by increasing the size of the targets as the distance to the observation point increases. As a rule of thumb, targets must be subtended about 0.5 degree with respect to the distance.
- About five targets spaced up to 300 meters from the camera are recommended. This is to allow accurate measurement of visibility up to 300 meters, which is considered an important range for highway applications.
- All targets must be visible in one screen.
- Targets must have black background and white stripes. The white stripes against the black background creates the strong contrast and edge information desirable for good visibility measurements. Anything other than white color can fail when the ground is covered with snow. It is important to recognize that white snow can create a strong false edge or contrast that can dominate the true edge or contrast information.

In our implementation, six targets were used, and two of them housed a constant light source. The targets were spaced 20m, 40m, 100m, 150m, 200m, and 300m. The target at 20m was installed for the initial dual-target approach introduced in Section III and does not contribute to the current computational model implemented in the field. However, it serves as a reference point for target search. The design of target with light source and the rest of the target dimension and pattern are shown Fig. 10 and 11, respectively.

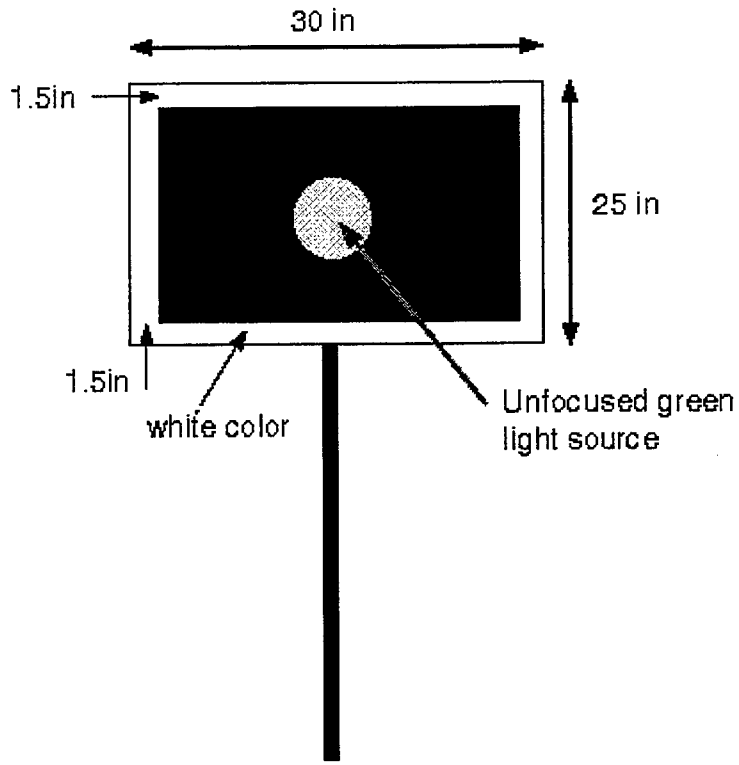

Figure 10: Target design for a constant light source.

C. Image Sampling and Software Tools

For sampling video images, a Snappy developed by the Plays Corp. was used. This digitizer is designed for still images and is connected through a printer port. The sampling time is about 6 seconds due to the slow speed of printer port. A customized, automated data collection program and a snapshot program were written using a C++ language for this research. Most image sampling was done at intervals of five minutes.

For the development of algorithms and implementation in the field, an Interactive Data Language (IDL) package was used as the basic language tool. The IDL provides a rich set of image processing routines that are very useful for implementing present application.

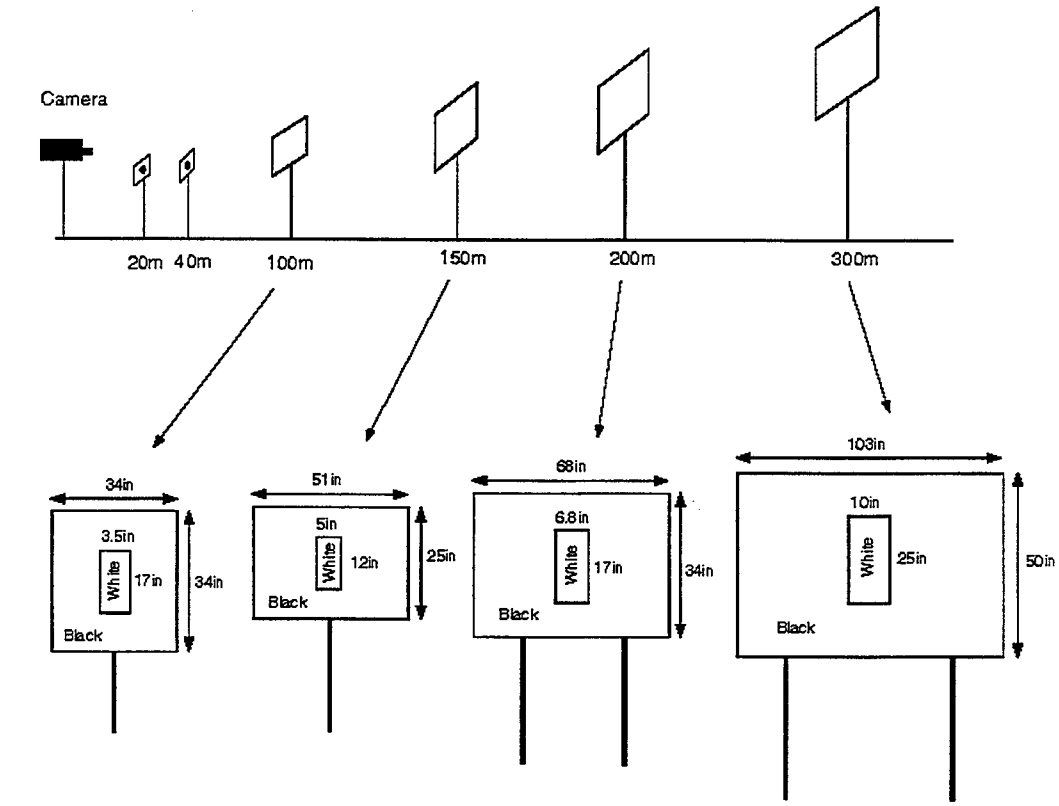

Figure 11: Target model used in the field implementation.

In order to remotely access the computer in the field, a modem and a LapLink from Traveling Software Co. were used. Initially, pcAnywhere from Symntec was used, but it caused frequent lock up of the remote computer and modem. The LapLink performed better under unstable phone lines and provided a better file transfer speed. In order to take advantage of the file transfer capability of LapLink, a JPEG file viewing program that also shows the visibility computed at the field was developed.

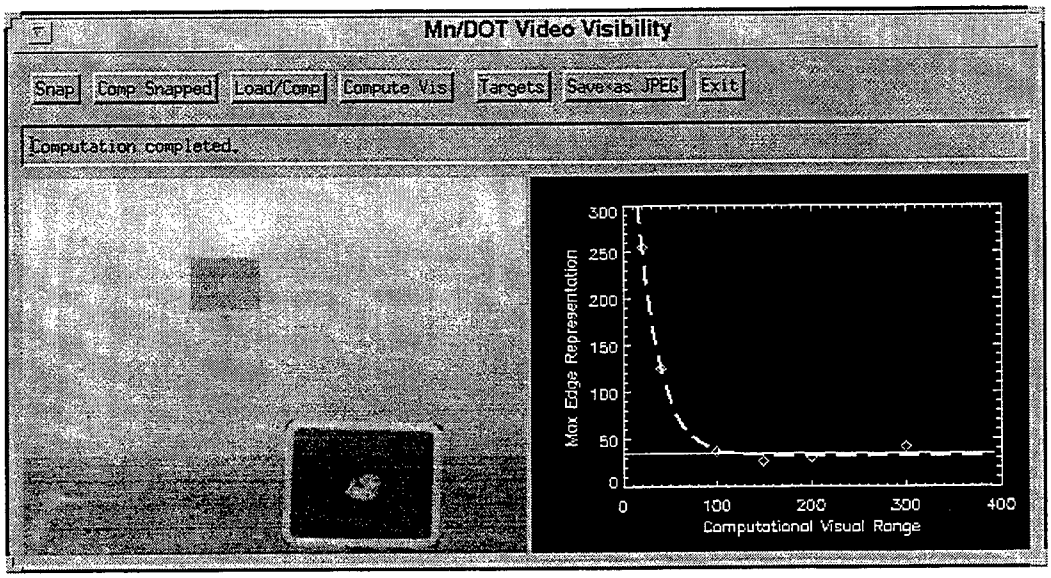

Figure 12: Sample screen of the visibility meter.

D. User Interface

The final form of user interface developed for this project is shown in Figure. 12. The primary goal was to develop a user-friendly interface which provides essential information that could lead to a better decision-making process with respect to visibility.

The image provided in the window allows manual verification. The graph shown in the right side window provides a mathematical modeling of the visibility which can be used to verify the correct curve fitting of the data.

The function of each button in the window is described below.

Snap Press this button to sample a picture using the Snappy digitizer. It digitizes and creates a 640X480 color bitmap-image, and then saves it as a file "tmpidl.bmp" which is later used by the other routines. This button

would be the first to press if one wishes to check the current visibility.

Comp Snapped Pressing this button will cause two actions. First, the color image grabbed by Snap (stored in "tmpidl.bmp") is converted to a gray scaled 320X240 image and displayed in the left side of the window. Next, visibility is computed, and the result is displayed using a pop-up message box.

Load/Comp This button loads an image from a storage selected by a user and computes its visibility. The result is displayed using a pop-up message box. This button is useful when the user wants to check images sampled in the past.

Compute Vis It computes the visibility of the image available in the current buffer. It can be used after **Comp Snapped** or **Load/Comp** to recheck the visibility.

Targets This button is used to see how the algorithm searches the targets. Pressing this button will display the searched result of the targets in the right side of the window. This routine is useful to check the target search-algorithm and to calibrate the camera angle to the targets.

Save as JPEG This routine converts the image available in the current buffer to a JPEG color image (320X240) and saves it at "C:\imagex\download.jpg". This file is created for the LapLink's automatic file synchronization utility to allow effective downloading to a local computer.

Exit Ends the current session.

The above program resides in the remote computer which is accessed though a LapLink remote control program from a local computer. Downloading of the captured image is done through the

LapLink's Automatic File Synchronization utility. Although images can be downloaded, there is no simple way to display the downloaded image along with the measured visibility at the local computer. Therefore, another utility program was created in order to decompress the downloaded JPEG image and display the measured visibility. A sample screen of this program is shown in Fig. 13

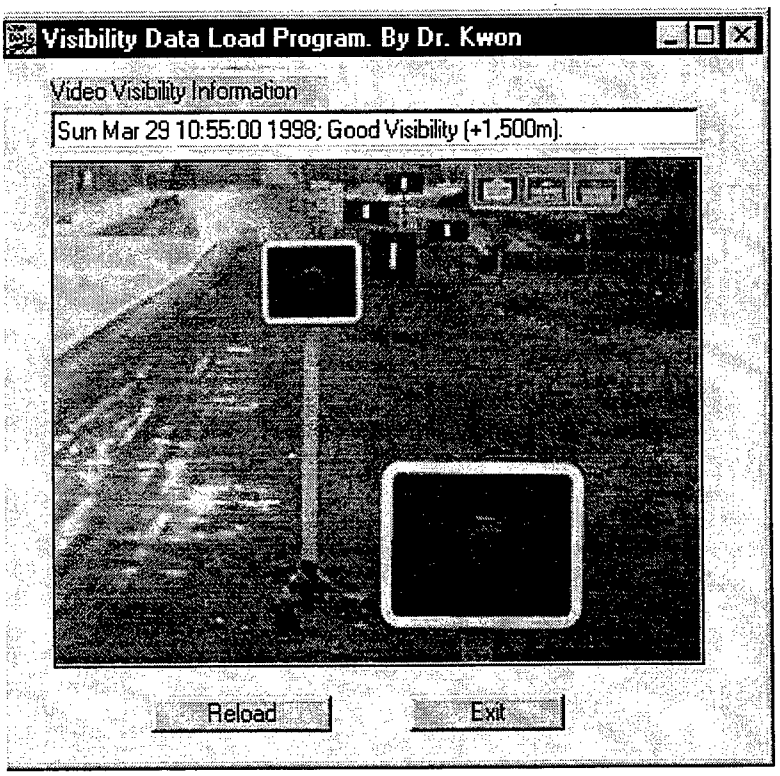

Figure 13: Customized visibility data and image loading program.

V. TESTS AND ANALYSES ON REAL-WORLD DATA

This section describes the tests and analyses of the developed visibility algorithms on real-world data. The first set of data was provided by Castle Rock Company and served as the resource for trying out various algorithms and developing new visibility evaluation techniques. Experimental results of Castle Rock's data are described in Subsection V.A. The field tests conducted are discussed in Subsection V.B.

A. Castle Rock Video Data

During the period from 1993 to 1995, Castle Rock Consulting firm tested several commercially available visibility sensors in a real world setting. The goal of this testing was to analyze the performance (accuracy and robustness) of each sensor against manual measurements. During this testing, video images were captured for verification and analysis purposes [5] and became the initial source of this study. In order to manually evaluate the visibility, the research team installed nine targets which were at distances: 5, 10.5, 20.1, 32.7, 67, 80, 100, 150, and 200 meters. The targets were numbered 1 though 9 for identification purpose. (See Fig. 3 in Section III.)

Before the analysis of Castle Rock's video data, a number of aspects must be taken into consideration. First, the manual measurements recorded in the data themselves had a large margin of error due to the limited number of targets. For example, at 150 meters, the error range is about 50 meters, since the next target available is at 200 meters. Second, the research team used identical target sizes for all targets regardless of the distance, such that targets located farther away were difficult to recognize or at least not given a fair chance of recognition rate. Third, in order to make a fair analysis, we wanted to have the data chosen from many different visual ranges and under different weather conditions. Ideally, this would include an equal number of samples from visibility near zero to two hundred meters from various weather conditions. Unfortunately, nature did not allow such an ideal data set. Indeed, the population of actual data was heavily biased, i.e., the data set was mostly concentrated in foggy conditions, and only one

day for snow and no data for rain. Forth, some of images were distorted by out-of-focus or water drops. However, these imperfect data helped develop a more robust algorithm.

As an initial test, the dual target approach developed in Section III was tested for all available images. The dual target approach worked well as long as the extinction coefficients were similar in both target areas. However, when the extinction coefficients were significantly different, it failed badly. We found that such conditions occur more frequently if the distance between two targets is larger. Another factor that influenced this method was distortion of image by water drops in the lens. If water drops appear at the target regions, a false contrast is measured for the affecting targets. Thus, the visibility computation significantly deviated from the real visibility. Later we realized that the log difference appears in Eq. (12) works as a noise or distortion amplifier for distorted images. After many experiments, we concluded that this method is not robust enough and not appropriate for video images.

After trying many ideas, we came to the conclusion that we need to develop a method that filters the localized errors. This direction led to a new theoretical model derived in Section III.C. In this approach, the main idea is to fit the imperfect data into a perfect model, such that the outliers of the data are ignored. The test of this idea was done through calculating the Sobel operator given in Eq. (23) in the target region (right side of image) and calculating the average which approximately represents the area under the curve of Eq. (24). From the data set, we selected the images that we consider ideal and constructed a table as shown in Table 1. Since this table is a one dimensional mapping, a polynomial model with a fifth order was used, i.e.

$$V = a_0 + a_1 S + a_2 S^2 + a_3 S^3 + a_4 S^4 + a_5 S^5 \qquad (33)$$

where a_0=*-0.00596*, a_1=*4.3541*, a_2=-0.07, a_3=0.000402, a_4=*-9.683*10^{-7}*, *and* a_5=*8.521*10^{-10}*. The graph of polynomial fitting is shown in Figure 14 which exhibits a near exponential relation.

Table 1: Idealized Parameters for Modeling.

Visibility	10	48	58	78	86.6	106	117	131	150	184	205	261	760
Sobel Estimate	150	245	270	280	289	311	325	342	360	377	396	412	485

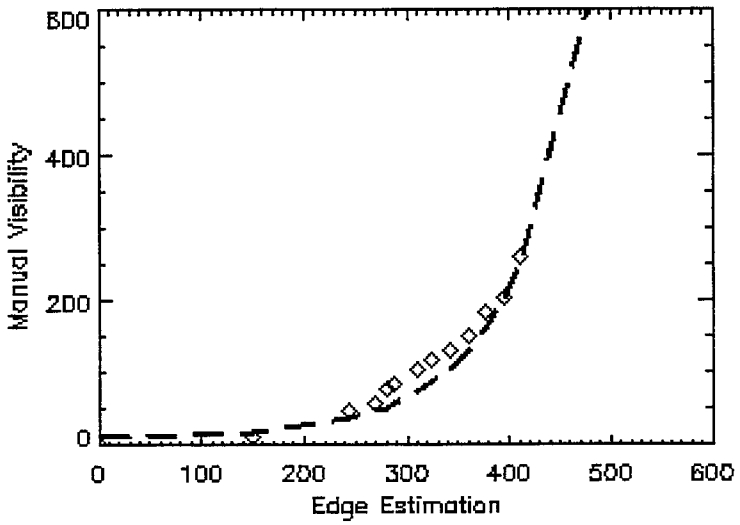

Figure 14:Polynomial visibility model for Sobel estimates.

The test results for Castle Rock's data are summarized in Tables 2 through 7 which include comparison of the visual ranges obtained from the commercial instruments. The column labeled Manual represents the visibilities measured by human observers in meters. The other columns correspond to visual ranges measured in meters by visibility sensors supplied by four companies, i.e. Viasala FD-12, Belfort Instrument's Model 6210, HSS's VR-301B-120, and Stern Löfving Optical Sensors' OPVD. Within the table, manual data should be considered most reliable (but

may not be most accurate), and should serve as the basis for the performance comparison. The symbol N/A indicates malfunction of the instrument at the time of measurement.

Tables 2 and 3 show the results of visibility tests on May 30 and June 6, 1994, respectively. Reduced visibilities on both days occurred due to fog. Notice that all of the video based measurements fall within the acceptable range. On the other hand, some of the commercial instruments such as the Stern clearly show a large error. For manual measurements, the highest measurable visibility was 200 meters, since the farthest target was located at 200 meters from the observation point. Hence, any visibility greater than 200 meters is shown as "200+".

Table 4 shows the test results for June 6, 1994 data. Again, the video approach shows reliable measurements. It can be noticed that the rest of instruments also fall within reasonable acceptable range except the Stern which appears to have been calibrated wrong.

Table 5 shows a case where the camera is out of focus. It happened between 5:00 - 5:10AM. Clearly the video approach slightly over estimates visibility due to the reduced edge information caused by the out-of-focus blur. Although the error is not drastic, this example illustrates importance of focusing during the sampling time for the video approach.

Table 2. Visibility test on May 30, 1994

Time	Manual	Video	Vaisala	Belfort	HSS	Stern
5:00 PM	200+	769	2923	1685	6912	836
5:05 PM	80 - 100	100	85	80	93	66
5:10 PM	32.7 - 67	44	44	61	50	32.7
5:15 PM	100 - 150	117	101	113	105	56
5:20 PM	150 - 200	165	143	152	134	68
5:25 PM	200+	795	1061	663	784	358

Table 3: Visibility test on June 5, 1994

Time	Manual	Video	Belfort	HSS	Stern
7:15 AM	200 +	746	N/A	1359	864
7:20 AM	80 - 100	106	163	158	271
7:25 AM	80 - 100	95	101	90	79
7:30 AM	100 - 150	128	132	106	91
7:35 AM	150 - 200	182	197	177	199
7:40 AM	200+	303	318	272	696

Table 4. Visibility test on June 6, 1994

Time	Manual	Video	Vaisala	Belfort	HSS	Stern
5:30 AM	100 - 150	99	N/A	124	105	256
5:35 AM	100 - 150	104	N/A	114	95	295
5:40 AM	100 - 150	96	N/A	105	88	279
5:45 AM	100 - 150	106	N/A	108	94	257
5:50 AM	100 - 150	94	N/A	95	79	272
5:55 AM	80 - 100	84	N/A	90	77	187
6:00 AM	80 - 100	86	N/A	84	69	162
6:05 AM	100 - 150	95	N/A	89	78	178
6:10 AM	100 - 150	107	N/A	97	80	227
6:15 AM	100 - 150	104	N/A	78	67	186
6:20 AM	80 - 100	88	N/A	69	58	153
6:25 AM	67 - 80	76	N/A	66	54	130
6:30 AM	100 - 150	116	N/A	92	85	169
6:35 AM	100 - 150	145	N/A	137	118	349
6:40 AM	150 - 200	246	N/A	190	170	1045
6:45 AM	150 - 200	165	N/A	144	133	522
6:55 AM	200+	1600	570	705	624	12108
7:00 AM	200+	995	432	392	413	864
7:05 AM	200+	405	214	208	210	783
7:10 AM	150 - 200	266	N/A	178	151	313
7:15 AM	100 - 150	133	102	112	110	358
7:20 AM	100 - 150	151	115	129	101	220
7:25 AM	100 - 150	141	129	149	127	292
7:30 AM	100 - 150	151	121	135	130	330
7:35 AM	150 - 200	164	151	156	154	284

7:40 AM	100 - 150	156	118	132	130	209
7:45 AM	100 - 150	242	105	126	111	176
7:50 AM	100 - 150	137	127	151	116	199
7:55 AM	150 - 200	152	256	235	219	738

Table 5: Visibility test on June 24, 1994.

Time	Manual	Video	Vaisala	Belfort	HSS	Stern
5:00 AM	100 - 150	72	126	153	144	267
5:05 AM	80 - 100	60	78	95	101	146
5:10 AM	80 - 100	72	127	112	99	123
5:15 AM	100 - 150	104	89	120	101	159
5:20 AM	150 - 200	152	170	206	189	181
5:25 AM	100 - 150	130	123	202	138	212
5:30 AM	80 - 100	67	77	119	77	120
5:35 AM	80 - 100	94	69	88	80	109
5:40 AM	80 - 100	77	54	72	68	106
5:45 AM	80 - 100	89	62	79	72	107
5:50 AM	80 - 100	91	66	85	77	130
5:55 AM	80 - 100	101	72	100	81	140
6:00 AM	150 - 200	177	151	191	184	236
6:05 AM	150 - 200	181	194	266	24	605
6:10 AM	150 - 200	219	212	283	241	447
6:15 AM	150 - 200	161	212	264	245	380
6:20 AM	200+	271	283	359	319	597

Note: Camera out of focused between 5:00 - 5:15 AM.

Table 6: Visibility test on June 27, 1994, Water drops on lens.

Time	Manual	Video	Vaisala	Belfort	HSS	Stern
4:40 PM	150 -200	109	199	221	219	390
4:50 PM	150 -200	84	140	142	133	100
4:55 PM	100 - 150	177	214	288	240	118
5:00 PM	150 -200	142	196	234	215	182
5:05 PM	100 - 150	115	155	168	145	93
5:10 PM	100 - 150	102	151	171	185	110
5:15 PM	100 - 150	95	109	126	98	85
5:20 PM	200+	290	399	357	297	180
5:25 PM	200+	306	590	708	618	274

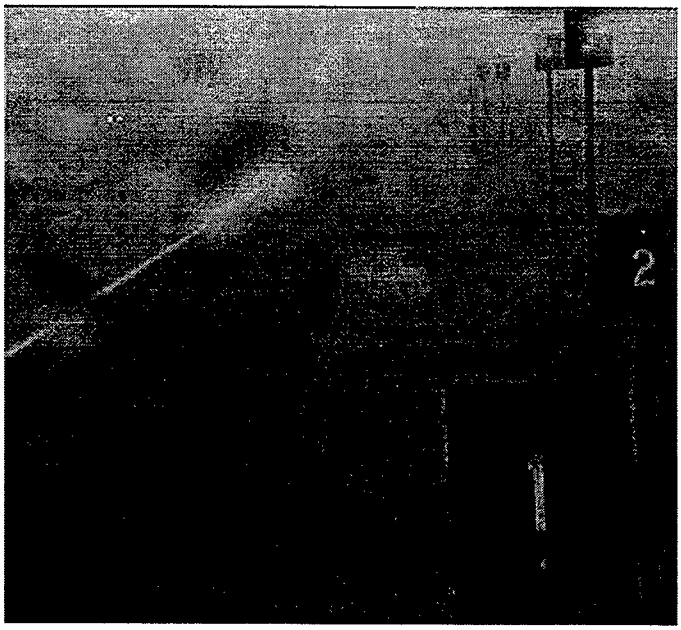

Figure 15: Example image that the lens is covered with water drops.

Table 6 reflects the cases in which the camera lens has water drops. The most severe example occurred at 4:50 PM and its image is shown in Fig. 15. The distorted camera image resulted in an over estimate of visibility. Therefore, this clearly shows that it is extremely important to protect the lens from water drops or other possible blocks. A more drastic problem can be expected when snow covers on the lens, since a large portion of the image could be lost . The visibility method applied here is based on filtering of outliers using average. This method works reasonably well even under the extremely distorted images as shown above, i.e., the visibilities measured by video are not that far removed from the manual measurements. However, we found that this method can be further improved by directly finding a fit function using the model given in Eq. (24). This method was implemented in the computer at the actual field.

Finally, we show the test results under snow conditions in Table 7. It can be clearly seen that all scattering based instruments tend to under estimate the visibility (i.e. show higher visibility) than human observers. On the other hand, the video based approach closely approximates the manual measurements. This is almost predictable, since the size of the snow particles are much larger and the distribution is not uniform, the scattering effect becomes more random and inconsistent. Another very important factor is that visibility is significantly reduced under snowy condition by the distortion of images sensed by the human visual system which can never be measured by the scattering effects. The advantage of the video based approach is apparent in that the method itself takes the degree of image distortion into consideration. It should be also mentioned that the basic polynomial model used in the video approach did not use the snow data at all, and yet the approach produced a reasonably good approximation to the manual measurements.

Table 7. Visibility test on February 25, 1994, Snow

Time	Manual	Video	Vaisala	Belfort	HSS
8:10 AM	150 -200	160	0	329	609
8:15 AM	100 -150	123	0	268	525
8:20 AM	200+ ??	139	0	296	476
8:25 AM	150 -200	153	0	323	500
8:30 AM	200+	183	0	271	477
8:35 AM	100 -150	128	0	238	343
8:40 AM	80 -100	105	0	214	325
8:45 AM	100 -150	122	0	244	405
8:50 AM	100 -150	111	0	262	475
8:55 AM	150 -200	179	0	0	656
9:00 AM	150 -200	140	0	300	615
9:05 AM	150 -200	167	0	291	581
9:10 AM	150 -200	118	0	343	798
9:15 AM	200+	206	0	581	1103
9:20 AM	200+	396	0	664	1376
9:25 AM	150 -200	343	0	454	1025
9:30 AM	150 -200	216	0	485	1140
9:35 AM	150 -200	250	0	474	767
9:40 AM	200+	340	0	431	760
9:45 AM	200+	185	0	442	858
9:50 AM	100 -150	194	0	317	674
9:55 AM	100 -150	112	0	235	347
10:00 AM	80 -100	123	0	177	351
10:05 AM	200+	258	0	359	664

Note for Table 7: Error in manual measurement at 10:00AM and the Vaisala and HSS sensors was not operating correctly.

B. Implementation and testing in the field

The daytime visibility algorithm was developed using Castle Rock's data, and modifications were made in the field implementation to accommodate the difference in targets and the sampling method. For nighttime, since no data was available, a new data set was collected and the appropriate algorithm was developed.

For real-world implementation, cameras can be shifted by wind or its own weight over time. Therefore, proper implementation requires a search of targets before visibility processing. A correlation coefficient algorithm [6] given in Eq. (33) was used for this purpose.

$$\gamma(s,t) = \frac{\sum_x \sum_y [f(x,y) - \bar{f}(X,Y)][w(x-s,y-t) - \overline{w}]}{\left\{ \sum_x \sum_y [f(x,y) - \bar{f}(x,y)]^2 \sum_x \sum_y [w(x,y) - \overline{w}(x,y)]^2 \right\}^{1/2}} \qquad (33)$$

where f is an M*N image, $s=0,1,2,..,M-1$, $t=0,1,2,...,N-1$, $\overline{w}$ is the average of the reference pattern w, $\bar{f}(x,y)$ is the average value of $f(x,y)$ in the region coincident with the current location of w. The correlation coefficient $\gamma(s,t)$ is scaled in the range -1 to 1. The detection result of actual targets using Eq. (33) for daytime targets and the night target is demonstrated in Fig. 16 and 17 respectively.

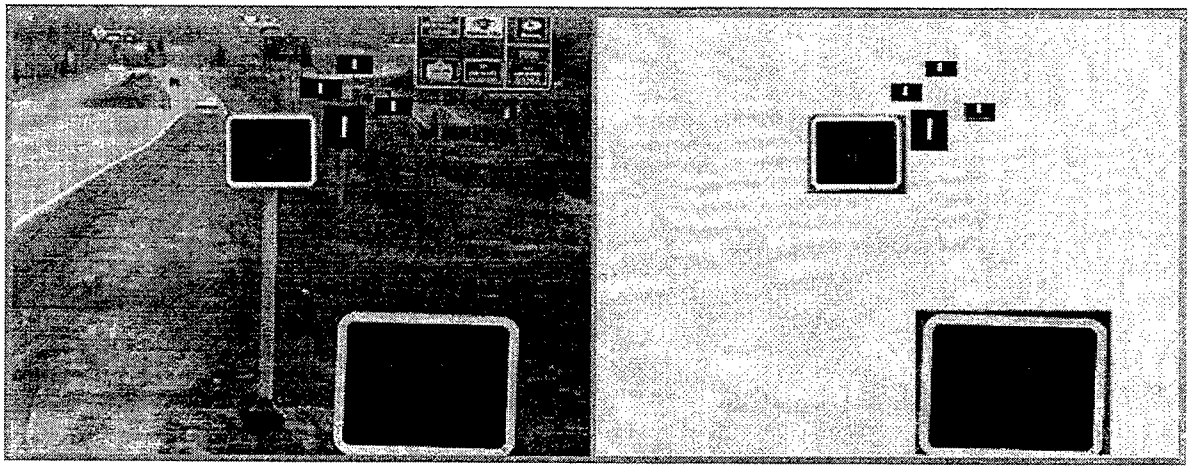

Figure 16: Example of daytime target detection.

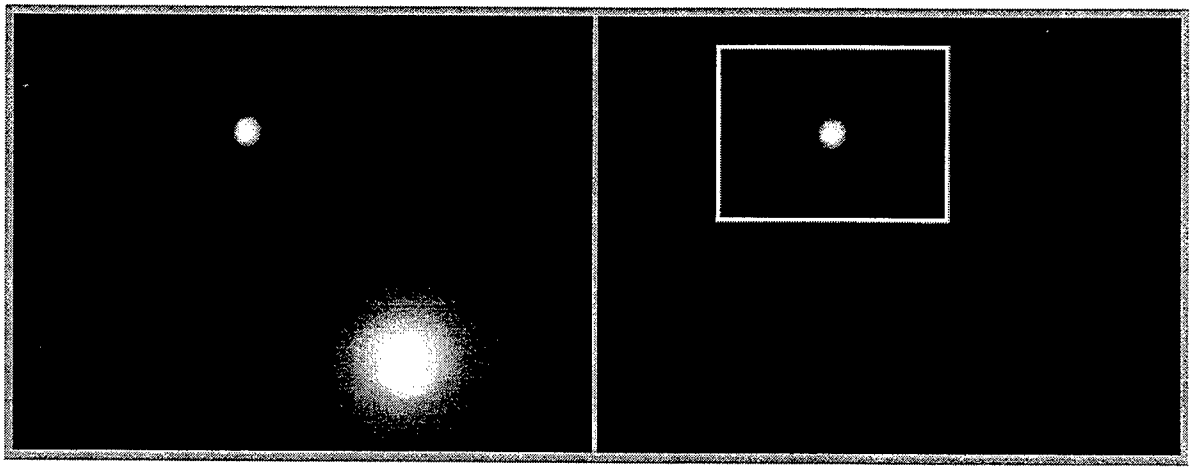

Figure 17: Example of nighttime target detection.

Since the goal of this research was to develop a practical methodology that could be reliably used in the field, the algorithm was continuously fine tuned through manual observations. A comparison study with commercial visibility sensors was not conducted, since the comparison was already done through Castle Rock's data in the previous subsection. Hence, we simply show the performance of the present implementation through the examples which we typically came across during the period of this research. In Fig. 18, good visibility where all targets can be clearly seen is shown. Notice that the exponential curve fit does not work on a clear day. This is

because identification of an object is no longer a function of atmospheric conditions but rather a function of its size. In general, we found that visibilities greater than 1,000 meters do not follow the standard exponential model. However, this characteristic is normal and adequate for transportation applications, since visibilities greater than 500 meters are of no concern.

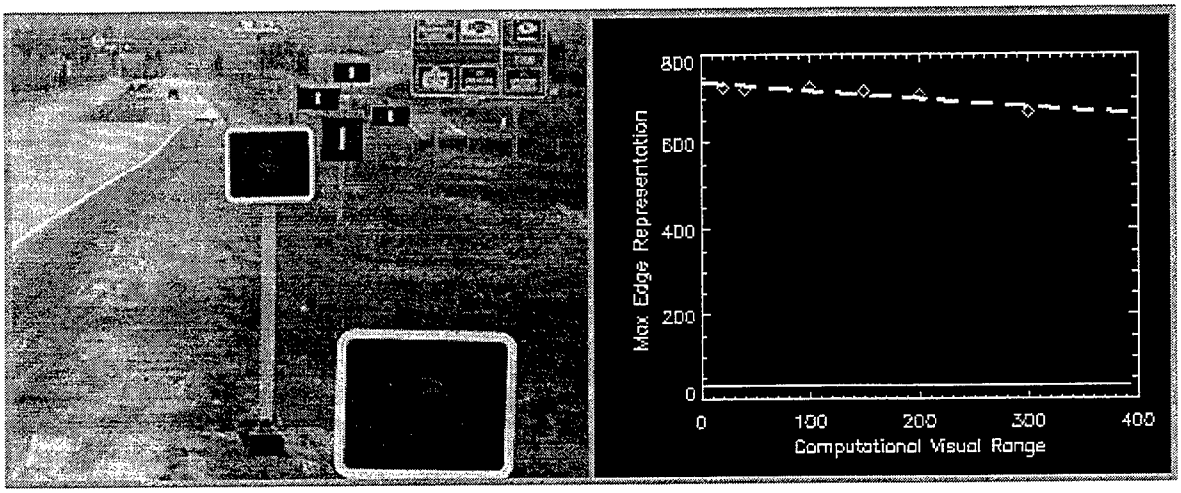

Figure 18: Good daytime visibility. Image taken at 11:50AM, June 7, 1997.

Figure 19 shows an example image of visibility 147 meters. Notice that this image follows the edge model developed in Section III.C very well. We found that visibilities less than 400 meters follow the model extremely well. From 400 meters to about 1,000 meters, the curve fit error slightly increases, but the model still works reasonably well and certainly operates within a tolerable range. However, after about 1,000 meters, the model fit error begins to drastically increase, and eventually the images no longer follow the exponential model.

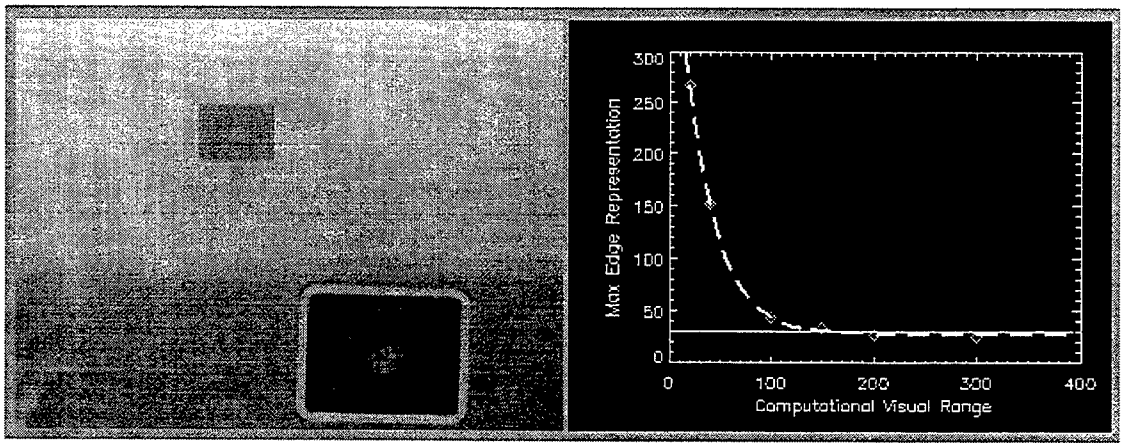

Figure 19: Visibility = 147 meters. Image taken at 8:35AM, July 25, 1997.

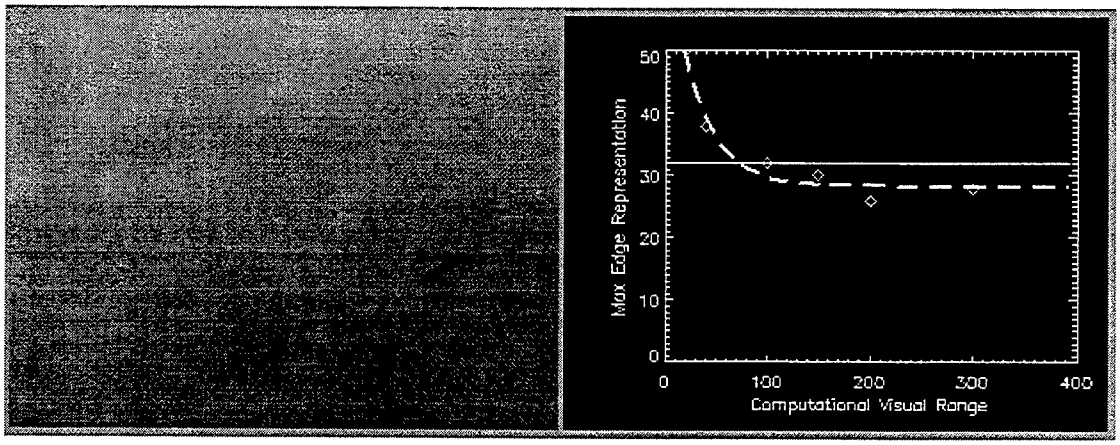

Figure 20: Visibility=73 meters. Image taken at 11:50AM, June 7, 1997.

Figure 20 shows an extremely bad visibility example which was recorded at 11:50 AM on June 7, 1997. The visibility was at 73 meters. Notice from the right side graph that, it closely follows the model. Although Fig. 20 looks less fit to the exponential model than Fig. 19, it is actually a better fit if they are plotted in the same scale. The key aspect is that the model works better as visibility gets worse, which is a desirable characteristic of a visibility sensor.

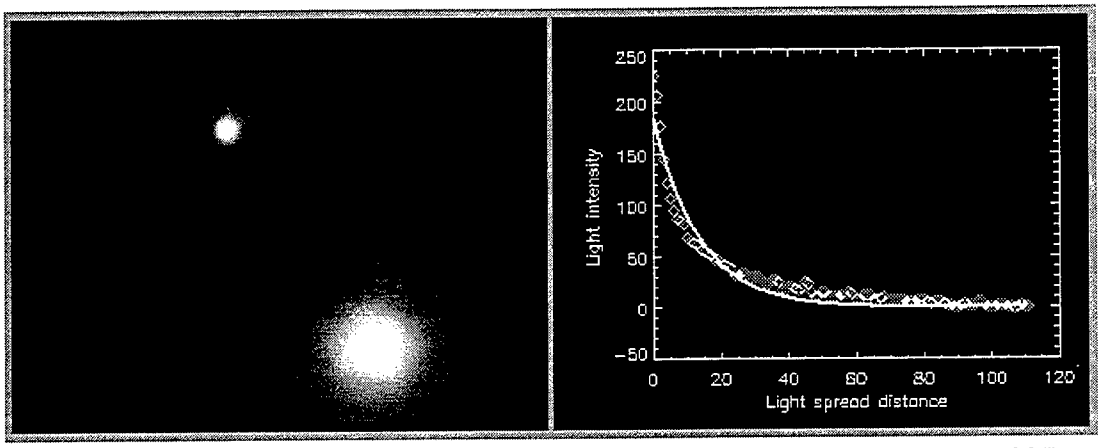

Figure 21: Night visibility=210 meters. Image taken at 10:20PM, Aug. 14, 1997.

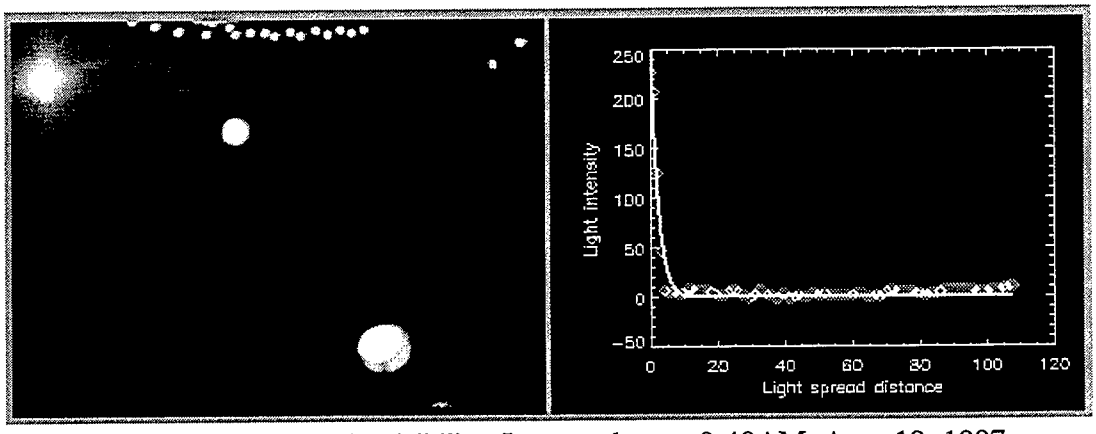

Figure 22: Good night visibility. Image taken at 0:40AM, Aug. 19, 1997.

Fig. 21 and 22 show night visibility examples. The graphs show the diffusion characteristics of each case, whereby as the visibility gets lower, the amount of light diffused from the saturated area becomes larger. This characteristic is used to compute the visibility. One possible problem for night visibility is the illumination of targets by the vehicles passing by, which can distort the amount of light diffused. In order to minimize this effect, it is recommended that the outside of the light source is painted non-glossy black. The height of the target should be high enough, so that it can avoid direct headlight hits. According to our experiments, the influence of light sources by vehicles crossing is minimal under low visibility, i.e. the lower the visibility, the less

influence. However, it was a significant source of distortion if the night was clear. Fortunately, such patterns can be easily detected and avoided by simple image processing techniques.

VI. DISCUSSION

This section discusses a number of issues related to video visibility learned during this research. It includes the existing problems, some solutions we found, related problems (such as blowing snow), and future directions.

A. Lens protection from dirts, snow, water drops, etc

One of the key prerequisites that the video camera based approach must try to achieve is to obtain a good image sample. The degree of distortion in the original image can significantly influence the performance of visibility accuracy as shown in Section V. The typical distortions we experienced include out-of-focus, motion blur, dirt, water drops, snow, frost, and blocking of targets by large objects. The next question then is how do we protect the image quality from the various types of distortions and obtain truthful images. To accomplish this, we took several steps. In order to minimize out-of-focus, we placed targets at extended distances and set the focus to infinity. Motion blurs were avoided by stabilizing the camera from the wind. This was achieved by covering the camera with a wind block box which was designed using aluminum. Water drops on a rainy day can be minimized by placing a protective shade at the top of the camera lens. Frost was minimized by the internal blower and heating block of the camera.

Protecting the lens from blowing snow was difficult to achieve. Due to the random direction of blowing snow, snow usually crept into the protective cover and eventually blocked the view of camera. When the protective lens was completely covered with snow, we often saw a totally black picture containing no image or information. One possible solution for this is applying compressed air into the lens. Although we did not install a compressed air blower for the present installation, it is highly recommend for future installation or study.

B. Visibility at day-to-night or night-to-day transition

Since our video based approach requires different algorithms for day and night, the algorithm must be able to detect day or night. We found that the transition does not occur gradually, but instead it occurs very abruptly. Once the time is completely emerged to day or night, the determination of it was not too difficult. This phenomenon helps widen the working range of the video based algorithm. However, we still needed some means to measure which algorithm would work better during the day/night transition time. We recommend that future implementations compute the correlation coefficient for both the day and night references and choose the larger value to determine which algorithm works better. The brightness of the transition area can be estimated by sampling day-to-night and night-to-day transition, from which the correlation coefficient can be computed. Another possible solution is using the weighted average of both the day and night measurement results, in which the weights are determined based on the correlation coefficients. However, this approach would require more computation time.

C. Reduced Visibility by vehicle generated snow clouds

The algorithms for this research have been developed for measuring atmospheric visibility which changes due to weather related atmospheric phenomena. However, there is another type of occurrence that can significantly influence visibility and can create dangerous driving conditions. When a small passenger car is behind a large truck on a snow covered road, the visibility seen by the passenger car can be almost zero if the truck generates a huge snow cloud (even if the atmospheric visibility is good).

During the data collection period, we observed the significance of blowing snow or snow clouds near the pavement. Indeed, we found that atmospheric visibility is rarely reduced by snow, but the snow cloud generated by vehicles or blowing snow near the surface very often severely

reduced the visibility. This type of reduced visibility usually occurs at a height of less than 1.5 meters from the ground. It was clear that the video based approach developed in this research would not be effective for this type of visibility because blowing snow can easily cover the lens and cannot locate the proper targets to reference. However, the following approach would be possible. A video camera is positioned at about three meters from the ground. Consecutive video images are then taken when a vehicle comes into the video screen and until it completely disappears. When a car is influenced by snow clouds, its overall shape will quickly disappear into the snow cloud. So if we measure the distance until the shape of vehicle is unrecognizable, that would give us the visibility that was reduced by the snow cloud. Although this method would require a great deal of computational time and memory because of the processing of many sequential frames, it will provide a solution for measuring visibility under vehicle generated snow clouds. Another approach that is low cost and attractive is counting the speed and size of snow particles using optical measurements. This could provide a good indirect measurement for the visibility generated by snow clouds. For more information on this method, please refer to references, [11,12].

D. Night visibility calibration

We found that manually measuring visibility at night is extremely difficult. The human eye can recognize light sources from greater distances at night than an object during the day. A simple example of this effect is that we can recognize the stars at night, but cannot recognize them during daytime. Because of this phenomenon, manual measurements usually end up severely under estimating (record higher than actual visibility) the visibility at night. Therefore, we recommend that night visibility be calibrated using scattering based sensors during fog which gives more consistent visibility readings. The calibration in this case means finding a multiplication factor in Eq. (30). Once the calibration is done during the fog, it can be used for snow or other conditions. At the present time, we are in the process of obtaining a scattering based visibility sensor and will eventually implement this calibration process.

E. Remote control

In order to remotely monitor the visibility and download the actual image, a remote control procedure must be implemented between the local and the field computer. The simplest way to accomplish this is to use a remote control software through an analog telephone line. In our case, a LapLink package developed by Traveling Software Co. was used. One difficulty we experienced was an unstable telephone line. The line was repeatedly connected and disconnected whenever the wind blew. This frequent line break caused a lockup of the remote computer or error in the modem. Eventually the line was fixed and all remote control functions worked flawlessly. The lesson we learned was that if the line is simply noisy, the modem will communicate with a slower speed, so it is still useable. However, if the line is unstable (meaning it randomly connects and disconnects), no remote control software was able to sustain the operation without an exception error which locks up the whole system or requires a direct input from the field computer. We also tested the pcAnywhere remote control package developed by Symantec Corp., but it caused an exception error at the field computer when the line was unstable.

F. Speed limit and visibility relation

If a driver sees a stopped vehicle in front in a single lane, the driver will break to stop his vehicle. The breaking distance will be greater if the vehicle is traveling at a higher speed. Also, before applying the breaks, the driver needs reaction time. During this reaction time, the vehicle will travel farther if its speed is higher. Let's assume that visibility is only 100 meters; the driver will not be able to see any vehicle stopped beyond 100 meters. Therefore, the safe speed limit in this case would be the speed that can bring the vehicle to a complete stop within 100 meters. The distance required for a complete stop to each speed is called a stopping sight distance and is computed using breaking distance and reaction time. The breaking distance at various speeds on wet pavement is shown in Table 8. The stopping distance computed using reaction time and breaking distance is shown in Table 9. From Table 9, we can create a simple rounded rule for a

speed limit model which could be used in practice. An example speed-model generated using 2.5 seconds reaction time is shown in Table 10.

Table 8: Breaking distance on wet pavements (Source from American Association of State Highway and Transportation Officials (AASHTO))

Assumed Speed (Mph)	Break Reaction		Friction Coefficient (f)	Breaking Distance on Level
	Time (sec)	Distance (ft)		
20	2.5	73.3	0.40	33.3
24-25	2.5	88.0-91.7	0.38	50.5-54.8
28-30	2.5	102.7-110.0	0.35	74.7-85.7
32-35	2.5	117.3-128.3	0.34	100.4-120.1
36-40	2.5	132.0-146.7	0.32	135.0-166.7
40-45	2.5	146.7-166.0	0.31	172.0-212.7
44-50	2.5	161.3-183.3	0.30	215.1-277.8
48-55	2.5	176.0-201.7	0.30	256.0-336.0
52-60	2.5	190.7-220.0	0.29	310.8-413.8
55-65	2.5	201.7-238.3	0.29	347.7-485.6
58-70	2.5	212.7-256.7	0.28	400.5-583.3

Table 9: Stopping sight distance

Speed (mph)	Stopping Sight Distance (meters)	
	Reaction Time (2.5sec)	Reaction Time (5sec)
25	45	73
30	60	93
35	76	115
40	95	140
45	117	167
50	141	196
55	164	225
60	193	260
65	221	293
70	256	334

Table 10: Suggested speed limit model

Weather	Visibility (meter)	Speed Limit (mph)
Clear	Above 270	70
Light Fog/ Flurry	190-270	60
Moderate Fog/ Light Snow	140-190	50
Dense Fog/Moderate Snow	95-140	40
Severe fog/Heavy Snow	45-95	25
Zero Visibility	Below 45	No Travel

VII. SUMMARY BY TASKS

This section describes the tasks proposed in the original proposal and discusses the results.

Task-1 Equipment Acquisition

Contact vendors and purchase the necessary equipment. A list of equipment and software includes a video camera, an image digitizer, a modem, a PC, remote access software, and miscellaneous items.

Results:

The purchased items can be divided into hardware and software tools. The hardware items purchased include:

- Compaq 4112 PC with 24M RAM and a VGA monitor.
- Iomega Zip Driver and Disks.
- Panasonic Color Video Camera (WV-CL354) with Heater and Blower Housing.
- Image Digitizer: Snappy.
- Constant Voltage Transformer.
- Modems: US Robotics Sportster and Motorola Voice SURFR
- Light Meter.

Software tools purchased include:

- Borland C++, Visual C++
- PC anywhere and LapLink
- IDL by Research Systems Inc.

During this period, data acquisition programs were developed and integrated into the overall system as an additional task. All programs were written for the Windows-95 interface.

Task-2 Development of Software

Develop algorithms and computer programs that derive visibility from the digitized video images. The techniques considered for the algorithm development include contrast measurement and analysis, noise level detection, discrete Fourier domain analysis, pattern identification, and statistical analysis.

Results:

For this task, a set of test data (images) was obtained from Castle Rock Consulting Co. The nature of this data is described in detail in Section V.A. Using this data, visibility algorithms were developed from SUN workstations at UMD using the IDL programming tools (IDL is a powerful scientific programming tool which have been used by many universities and government agencies). The resulting algorithms are described in Section III of this report.

Task-3 Data Acquisition and Measurement Verification

Collect data using the video camera under varying visibility conditions: fog, snow, and rain. Verify and refine the visibility measured by the system.

Results:

A data acquisition system was installed at the Thompson Hill research site using the equipment and software tools purchased and developed in Task-1. This site is well known for reduced visibility problems and was recommended by Mn/DOT. Data was collected from Oct. 1996 to Dec. 1997 and saved in Zip disks. The visibility algorithm developed from Task-2 was installed in the field computer at this time for verification and continuous refinements. The final result of the algorithm was shown in Section III.C of this report. The data collection task was extended from the original plan of Oct. 31, 1997 to July 15, 1998 due to an additional need for collecting night data. Additional night data was successfully collected and contributed to the development of a new nighttime algorithm shown in Section III.C.

Task-4 Installation of Remote Access Capability

Install and test remote access software. Installation of this utility provides a mechanism that transfers data to remote users. A user may dial-in to the modem attached to the system and may receive data for visibility and the corresponding video information. The received video information can then be used for manual verification and also for other purposes such as traffic control.

Results:

For this task, two remote control programs, LapLink by Traveling Software Co. and pcAnywhere by Symantec Corp., were purchased and installed. After extensive testing, we concluded that LapLink was more stable and appropriate for the given application. PcAnywhere frequently locked up the modem in the field. The installed remote control program was then used to connect to two other programs (Mn/DOT Video Visibility and Visibility Data Load Program) developed for this project. These two programs were described in Section IV.D User Interface.

The overall system was delivered and installed in the field. Using the overall system is very simple and works as follows: (1) Connect the field computer using LapLink through a standard modem, (2) Double click on the IDL icon, (3) Type in 'video_vis' at the IDL command line which brings up the window shown in Figure 12, (3) Click on the 'snap' button to take a picture and then click on the 'comp snapped' button to compute the visibility. The present visibility will then be displayed in a pop-up message box. After checking the visibility, the user may download the image or simply close the windows. Downloading the captured image is also very simple. Simply click on the 'Save as JPEG' button and then click on the LapLink's Automatic File Synchronization icon. The downloading of the captured image then will be automatically performed. Clinking the 'Visibility Data Load Program' icon on the desktop of local PC will display the window shown in Figure 13 which displays the measured visibility and the downloaded image.

VIII. CONCLUSIONS

The goal of this research was to develop a good theoretical basis and a practical method for measuring visibility using video cameras. Several new algorithms were developed and tested. The most practical algorithm for daytime was the one introduced in Section III.C which is based on an edge decay model. The edge information of an image provided information on how far one can see and recognize an object of a specific size. For night time visibility, we developed a new diffusion model that can be effectively fitted into an image with a constant light source. These new concepts and algorithms were extensively tested using the data collected by a previous study directly in the field, and proven effective. However, for night time, a fine tuning of the multiplication factor in Eq. (30) or a mapping function in Eq. (31) is necessary because it was solely determined by manual measurements which tend to be unreliable at night. This study is presently underway and will be reported in the future.

Through this study, we noticed that reduced visibility in Minnesota occurs mostly due to two factors, fog and snow. Let us consider fog first. Fog usually forms under certain geographical characteristics with a combination of special atmospheric conditions. Therefore, fog does not occur at random and tends to occur in certain isolated areas. Spotting such areas is not that difficult in Minnesota due to its frequent occurrence. This leads to a recommendation that visibility sensors should only be placed in problem areas. The author believes that the developed video based approach is particularly suitable for remote areas where reduced visibility frequently occurs and the visual information is very important. Let us now consider snow. Throughout this study, the author observed visibility under many snow storms and found that atmospheric visibility is rarely reduced to below 200 meters. This observation is based on manual measurements at a stationary position. It may sound strange, but the intelligence of human visual system seems to recognize noisy objects (distorted by snow particles) reasonably well. However, the visibility sensed by a driver of a moving vehicle is much lower than the stationary observation. This is mainly because as the vehicle moves, snow particles begin to hit the front window shield and block the clear view of objects. Moreover, the perceived visibility is further

decreased as the speed of the vehicle increases, due to the increased hit rate of snow particles. The problem is compounded at night by snow particles reflected off vehicle's head light and other light sources. Since these factors severely reduce the driver's perceived visibility beyond the atmospheric visibility, we recommend them to be included in visibility computation for snow. Further consideration should also be given to the vehicle generated snow clouds and blowing snow. These generally occurs near ground (within 2 meters from ground) and severely influences the driver perceived visibility.

In conclusion, the video based approach developed in this project is an effective tool for measuring atmospheric visibility for all types of weather conditions. The method is reliable and cost effective. It provides a means of verifying the visibility through visual images, and all areas with visibility problems in Minnesota already have video cameras in place. One limiting factor observed was a good design of video cameras from which blowing snow and rain can be blocked or prevented from getting into the lens. However, this problem is considered solvable with new camera design techniques. In the case of evaluating driver perceived visibility, the main discrepancy occurs under snow as described above. A further study is recommended for proper quantization of such effects.

REFERENCES

[1] American Meteorological Society. *Glossary of Meteorology*, 1989.

[2] W. E. Knowles Middleton, *Vision Through Atmosphere*, 1968, University of Toronto Press.

[3] E. J. McCartney, *Optics of the Atmosphere: Scattering by Molecules and Particles*, John Wiley & Sons, New York, 1976.

[4] S. Q. Duntley, "The Reduction of Apparent Contrast by the Atmosphere," *J. Opt. Soc. Am.*, vol 38, 179-191.

[5] Castle Rock Consultants, *Environmental Sensor Systems for Safe Traffic Operations*, U.S. Department of Transportation, Federal Highway Administration, Research and Development, Turner-Fairbank Highway Research Center, Publication No. FHWA-RD-95-073, 1995.

[6] R. C. Gonzalez and R. E. Woods, *Digital Image Processing*, Addison-Wesley Publishing Company, Reading, Massachusetts, 1993.

[7] E. L. Hall, *Computer Image Processing and Recognition*, Academic Press, London, UK, 1979.

[8] C. A. Douglas and R. L. Booker, *Visual Range: Concepts, Instrumental Determination and Aviation Applications*, U.S. Department of Transportation, Systems Research and Development Service, Report No. FAA-RD-77-8, Washington, D.C. 20590, 1977.

[9] S.Q. Duntley, R.W. Johnson, J.I. Gordon and A.R. Boileau, *Airborne Measurements of Optical Atmospheric Properties at Night*, University of California, Scripps Institution of Oceanography, Visibility Laboratory, SIO Ref 70-7, AFCRL-70-0137, NTIS No AD 870 734, 1970.

[10] R.W. Johnson, W.S. Hering, and J.E. Shields, *Automatic Visibility & Cloud Cover Measurements with a Solid-State Imaging System*, University of California, Scripps Institution of Oceanography, Parine Physical Laboratory, SIO Ref 89-7, MPL-U-26/89, GL-TR-89-0061, 1989.

[11] R. A. Schmit, "Measuring Visibility in Blowing Snow," Snow Removal and Ice Control Research, Spec. Rep. 185. Proc. 2nd International Symp, National Academy of Science, pp.

200-207, May 15-10, 1978.

[12] R. D. Tabler, "Using Visual Range Data for Highway Operations in Blowing Snow," Optical Engineering SPIE, vol. 23, pp. 55-61, Jan/Feb, 1984.

[13] Biral, "Operation and Maintenance Manual for the VPF-700 Series of Sensors," Biral HSS Sensors, United Kingdom, 1997.